Clinical Neurophysiology 130 (2019) 976–985

Contents lists available at ScienceDirect

Clinical Neurophysiology

journal homepage: www.elsevier.com/locate/clinph

Redaction of false high frequency oscillations due to muscle artifact improves specificity to epileptic tissue

Sijin Ren [a], Stephen V. Gliske [a,b], David Brang [c], William C. Stacey [a,b,*]

[a] Department of Neurology, University of Michigan, USA
[b] Department of Biomedical Engineering, Biointerfaces Institute, University of Michigan, USA
[c] Department of Psychology, University of Michigan, USA

ARTICLE INFO

Article history:
Accepted 16 March 2019
Available online 11 April 2019

Keywords:
High Frequency Oscillations
Muscle artifacts
Algorithms
Epilepsy
EEG

HIGHLIGHTS

- Muscle artifact is easily mistaken for intracranial HFOs, especially in the temporal lobes.
- Two methods are presented to identify and redact these "EMG-false-HFOs".
- Removal of EMG-false-HFOs improves HFO specificity to epileptic tissue.

ABSTRACT

Objective: High Frequency Oscillations (HFOs) are a promising biomarker of epilepsy. HFOs are typically acquired on intracranial electrodes, but contamination from muscle artifacts is still problematic in HFO analysis. This paper evaluates the effect of myogenic artifacts on intracranial HFO detection and how to remove them.
Methods: Intracranial EEG was recorded in 31 patients. HFOs were detected for the entire recording using an automated algorithm. When available, simultaneous scalp EEG was used to identify periods of muscle artifact. Those markings were used to train an automated scalp EMG detector and an intracranial EMG detector. Specificity to epileptic tissue was evaluated by comparison with seizure onset zone and resected volume in patients with good outcome.
Results: EMG artifacts are frequent and produce large numbers of false HFOs, especially in the anterior temporal lobe. The scalp and intracranial EMG detectors both had high accuracy. Removing false HFOs improved specificity to epileptic tissue.
Conclusions: Evaluation of HFOs requires accounting for the effect of muscle artifact. We present two tools that effectively mitigate the effect of muscle artifact on HFOs.
Significance: Removing muscle artifacts improves the specificity of HFOs to epileptic tissue. Future HFO work should account for this effect, especially when using automated algorithms or when scalp electrodes are not present.

1. Introduction

Over the past 20 years, the role of High Frequency Oscillations (HFOs) in identifying epileptic tissue has been the subject of a great deal of research (Jacobs et al., 2012). HFOs are brief (<100 ms), low amplitude waveforms seen on EEG in the 80–500 Hz band, which is well beyond the range typically visible in clinical studies. Therefore, all HFO research requires analysis using techniques to isolate these high frequency signals from the overlying, traditional EEG signals that have strong spectral power under 30 Hz (Worrell et al., 2012). The majority of clinical research is based upon identifying elevated rates of HFOs on intracranial EEG (Zijlmans et al., 2012). Several studies have shown that brain regions with high levels of HFOs are likely to be within the Epileptogenic Zone (EZ), a theoretical region of tissue that, when removed surgically, allows patients to become seizure free (Frauscher et al., 2017; Gloss et al.,

* Corresponding author at: Department of Neurology, University of Michigan, 1500 E. Medical Center Drive, SPC 5036, Ann Arbor, MI 48109-5036, USA. Fax: +1-734 936 5520.
E-mail addresses: sijinren@umich.edu (S. Ren), sgliske@umich.edu (S.V. Gliske), djbrang@umich.edu (D. Brang), william.stacey@umich.edu (W.C. Stacey).

https://doi.org/10.1016/j.clinph.2019.03.028
1388-2457/

2014; Holler et al., 2015). However, identifying HFOs is a very laborious task, requiring many hours to process a single 10-min epoch of data manually. This difficulty has led several groups (Blanco et al., 2010; Crepon et al., 2010; Gliske et al., 2016; Liu et al., 2016; Navarrete et al., 2016; Roehri et al., 2017; Zelmann et al., 2012) to develop automated HFO detection algorithms, many of which were validated to be as accurate as human reviewers and process the data exponentially faster. Accurate identification of true (i.e. cerebrally-generated) HFOs is paramount for any detector, whether human or automated.

Both manual and automated HFO detection schemes have been based upon reviewing each channel independently (Worrell et al., 2012). This allows unbiased interpretation, but it also risks misinterpreting non-physiological activity as HFOs. One of the most important type of "false HFO" is caused by fast transients in the EEG, which can generate ringing oscillations after filtering due to a processing artifact known as Gibbs' phenomenon (Benar et al., 2010). Manual reviewers and recent computational algorithms have developed strategies to avoid these false positive detections (Gliske et al., 2016). However, there is one type of potential false HFO that cannot be avoided reliably when processing isolated channels in this manner: muscle artifacts.

One of the benefits of analyzing intracranial EEG in traditional frequencies (<30 Hz) is that the effects of muscle and movement artifact are greatly diminished, especially in comparison with the amplitude of the standard EEG waveforms under 30 Hz. However, this benefit is not as prominent when compared with the low amplitude activity at higher frequencies. Muscle activity produces high amplitude, broadband electrical signals that are sometimes large enough to be visible intracranially and appear very similar to HFOs. This phenomenon has been described previously in other areas of research, such as ocular-muscle electromyogram producing false gamma oscillations (which look like the gamma of normal cognitive processing) (Kovach et al., 2011), or chewing artifact producing false HFOs intracranially (Otsubo et al., 2008). Many past HFO studies have tried to mitigate this effect by restricting analysis to slow wave sleep when movement artifacts are less likely. Despite this common practice, there are several reasons for developing this algorithm: (1) automated detectors are required in longer studies, and no HFO detection algorithm has addressed this effect explicitly; (2) there still are some artifacts during slow wave sleep, and manual review is often required to affirm the absence of EMG activities; (3) in prolonged recordings there are many HFOs seen in other behavioral states, which are ignored when the analysis is limited to slow wave sleep; (4) many intracranial EEG studies do not use simultaneous scalp electrodes, which makes it difficult to identify muscle artifact; (5) there has been very little prior work demonstrating the effect of direct intracranial projections of myogenic waveforms and how to recognize them visually. Thus, in this study we seek to quantify and mitigate the effect of muscle activity on HFO detections with an automated algorithm.

Starting with a previously-validated HFO detector that removes intracranial artifacts from sharp transients (Gliske et al., 2016), we first generate a list of intracranial HFOs from interictal periods. We then develop two methods to redact detections that were generated by scalp EMG artifact: an EMG detector on the scalp EEG channels (to be used when scalp EEG is available), and a feature-based detector on the intracranial EEG that does not require any scalp EEG recordings. Using these automatically identified false positive detections, which we call EMG-false-HFOs, we characterize the spatial distribution of EMG contamination in intracranial recordings. Finally, we evaluate the clinical significance of removing 'EMG-false-HFO', and find that muscle artifacts greatly affect HFO interpretation of a subset of patients.

2. Methods

2.1. Data acquisition

Intracranial EEG was obtained during routine intracranial monitoring in preparation for epilepsy surgery in patients with intractable seizures. All patients consented to have their deidentified data utilized for research and the study was approved by each institution's review board. Twenty-seven patients from the University of Michigan (UM) and four from Mayo Clinic (MC) were included in the study. For intracranial EEG, 15 UM patients were recorded with a Blackrock acquisition system (Salt Lake City, UT) with sampling rate of 30,000 Hz and downsampled to 5000 Hz, the other 12 patients were recorded with a Natus Quantum acquisition system sampling at 4096 Hz (Gliske et al., 2018), and the 4 MC patients were sampled at 32 kHz with a Neuralynx acquisition system (Bozeman, MT) and downsampled to 5000 Hz (Worrell et al., 2008). Simultaneous scalp EEG was available on 21 of the UM patients (10 Blackrock, 11 Quantum) using the same sampling rate and amplifier as the intracranial study. Data analysis was restricted to periods that were greater than 30 min before and after any seizures that had been marked in the standard clinical reports. In each analysis described below, all patients from this set that contained the necessary data were used.

2.2. HFO detection algorithm

The initial HFO detections were obtained using a previously validated algorithm, which utilizes a highly sensitive detector (Staba et al., 2002), then redacts periods containing sharp artifacts or widespread events that are unlikely to be cerebrally-generated HFOs (Gliske et al., 2016). The resulting detections are referred to as qHFOs, which have high agreement with human reviewers for removing non-physiological artifacts (Gliske et al., 2018; Li et al., 2018). Of note, like all other previous HFO detection algorithms, it does not have a specific mechanism to redact artifacts caused by scalp EMG.

2.3. EMG detectors

Two independent methods were then utilized to identify EMG-false-HFOs in those qHFO detections, one based upon scalp EEG and one with only intracranial EEG.

2.3.1. EMG detector for scalp channels

When simultaneous scalp EEG is available, a straightforward way to identify periods in which muscle artifact is likely to have caused HFOs is to determine when HFOs occur at the same time as EMG in scalp EEG channels. Clinicians are trained to identify periods of muscle artifact in the scalp: the high-frequency, high-amplitude signals stand out from the background and are readily identifiable by eye, and the EEG is often ignored during such periods. To recapitulate this process with an automated algorithm with HFOs, we first mimic the clinical approach of identifying muscle artifact on the scalp. To do this, we used a line length algorithm (Gardner et al., 2007) to detect the EMG artifacts directly in the scalp channels, which can then be used to redact periods of unreliable intracranial EEG similar to the artifact rejection in the qHFO algorithm (Gliske et al., 2016).

The line-length detector was run on 10-min-long, non-overlapping epochs of scalp EEG. Each channel was referenced to the common average of all scalp EEG channels and decimated to 500 Hz after low pass filtering at 250 Hz. A comb filter at 60 Hz and its harmonics was then applied, using Matlab's 'fdesign.comb ('notch',...)' function (Mathworks). The filtered signals were then

analyzed by computing the amplitude range and line length (sum of the absolute values of the differences between consecutive samples) using a sliding window of 0.2 sec, with an overlap of 0.1 sec (Fig. 1). The algorithm first calculated an estimate of the line length of the background EEG activity by averaging forty-nine 0.2-sec windows randomly selected from the 10-min epoch, which we called the baseline. Then the line length was calculated for the entire epoch at each location of the sliding window. We computed the ratio between each line length value of the sliding window and the baseline. If a window's line length was less than twice the baseline, we determined that there was no muscle artifact and updated the baseline with that value by discarding the oldest of the 16 samples in the baseline and recalculating the baseline. If the value was between 2 and 2.5 times the baseline, there was no artifact. If the value was greater than 2.5 times the baseline, we used another measure to distinguish between muscle activity and other phenomena with large line length, such as epileptic spikes. We did this by first subtracting the mean of baseline from the line length value, then dividing the resulting value by the range of the samples in the sliding window. If this ratio was greater than 6, the corresponding samples were classified as muscle (Fig. 1B). These parameters were chosen based upon training in one patient during a 10-min period of chewing artifact. As the sliding windows generate two different values for each 0.1-sec, the average of these two values is used to determine if the current 0.2-sec window will be marked as muscle artifact. The calculation generates a new average every 0.1 sec, resulting in a list of 0.1-sec windows in which there is potential muscle artifact in individual channels of the scalp EEG. The final determination of the presence of scalp EMG artifact was made by identifying all 0.1-sec windows in which at least 2 channels were marked as likely EMG (Fig. 1C).

2.3.2. Scalp EMG detector validation

The detector was validated by comparing results with a human reviewer with expertise in reading EEG. The reviewer viewed the entire scalp EEG using standard 10–20 electrodes for three 10-min epochs from 3 different patients other than the patient used for tuning, and marked every time in which there was any muscle artifact. These markings were used as the gold standard for assessing the algorithm performance.

Note that labeling all HFO detections time-locked with EMG detections as artifacts may result in real HFOs being redacted due to random coincidence between brain oscillations and EMG. This is especially prominent in some patients who have continuous muscle activity lasting for prolonged periods. In addition, all intracranial electrodes are not necessarily affected by focal EMG artifact, e.g. they can be distant or contralateral to the location of the EMG. Therefore, it is necessary to determine whether a specific intracranial electrode is affected by the EMG artifact from each individual scalp EEG electrode. We evaluated the correlation between HFOs detected intracranially and the surface EMG artifacts. For each pairing of intracranial and scalp electrodes, we determined the proportion of HFOs on the intracranial channel that were coincident with EMG on that scalp channel. We divided this ratio by the total proportion of time in which that scalp electrode had EMG artifact. If the HFOs are not being produced by the EMG in that scalp channel, we expect the coincidence to be random, and this ratio, which we call the EMG Suspicion Ratio, to be equal to 1. In contrast, if HFOs tend to be produced by the EMG, then the ratio will be much higher. We plotted the histograms of these values for 20 patients individually and found many patients with bimodal distributions, suggesting some channels with and some without correlation to scalp EMG. We found that a threshold of 5

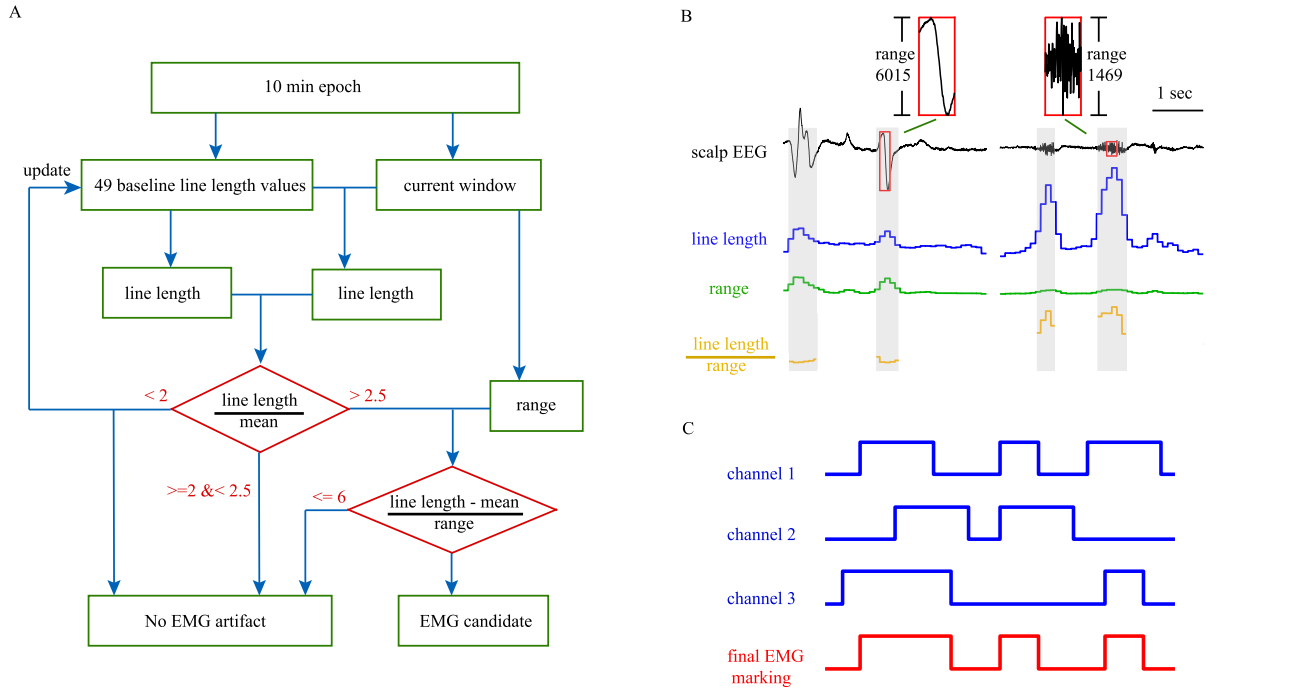

Fig. 1. Scalp EMG detector algorithm. A. Algorithm flow chart, based upon training in a single patient, identifies when line length is high compared with the mean line length and the amplitude range. The latter stipulation avoids misclassifying epileptic spikes. B. An example of the algorithm process comparing the results of a spike (left) with a muscle artifact (right). Both have line length greater than 2.5 times the baseline, but the relatively high amplitude of the spike correctly distinguishes it from EMG. Note that EMG artifact with amplitudes similar to spikes will be classified correctly, because their line length is also much higher. C. Final classification as EMG artifact requires at least two channels to have potential EMG at the same time. This assessment is made as a binary classification, indicating all 0.1 sec windows in which there is EMG artifact on the scalp.

provided a good separation of the bimodal distributions (values between 3 and 10 generated essentially identical results). Thus, we determined that any intracranial-extracranial electrode pair with EMG Suspicion Ratio > 5 was likely to indicate a real association between HFO detections and EMG artifact, i.e. that the scalp EEG was likely producing EMG-false-HFOs. We defined an intracranial EMG-false-HFO whenever EMG is detected on the paired scalp channel(s).

2.3.3. Identifying EMG-false-HFO based on intra-cranial waveform features

As not all patients with intracranial EEGs also have simultaneous scalp recordings, we also developed a method to identify EMG-false-HFO using only the intracranial EEG, based on their intracranial waveform features. All available patients were evaluated with this intracranial detector, and in those patients that also had scalp EEG we were able to compare the results of the two independent detectors. Previous studies have shown that EMG artifacts are generally wide-band events (Otsubo et al., 2008) whereas neural HFOs tend to produce isolated 'islands' in time-frequency maps (Fig. 2c). We decided to use wavelet transforms to identify these spectral islands and distinguish them from wideband artifacts. Wavelets are suitable given the potential nonstationarity of the waveforms ((Liu et al., 2016), Also see Fig. 2c). We applied analytic Morse wavelets (symmetry = 3, time-bandwidth product = 60) to a 100 ms signal (band-pass filtered 80–500 Hz) centered around each qHFO detection. This outputs a matrix with entries representing a range of spectral power at every time point. Normalized Shannon entropy of the entries corresponding to frequencies within 80–500 Hz is used as a quantification of 'irregularity' in the time-frequency spectrum, where high entropy indicates lack of clear isolated 'islands'. In order to automatically identify periods of high entropy, we used a Bayesian classifier in Matlab (Mathworks) (fitcnb(. . .,'Distribution','Kernel') to determine the threshold by which to identify the difference produced by either HFO or EMG in the time-frequency spectrum. We trained this classifier by comparing with human-labeled HFO detections, with the initial, conservative parameter for the Bayesian 'prior' set to 0.3 to be considered as EMG.

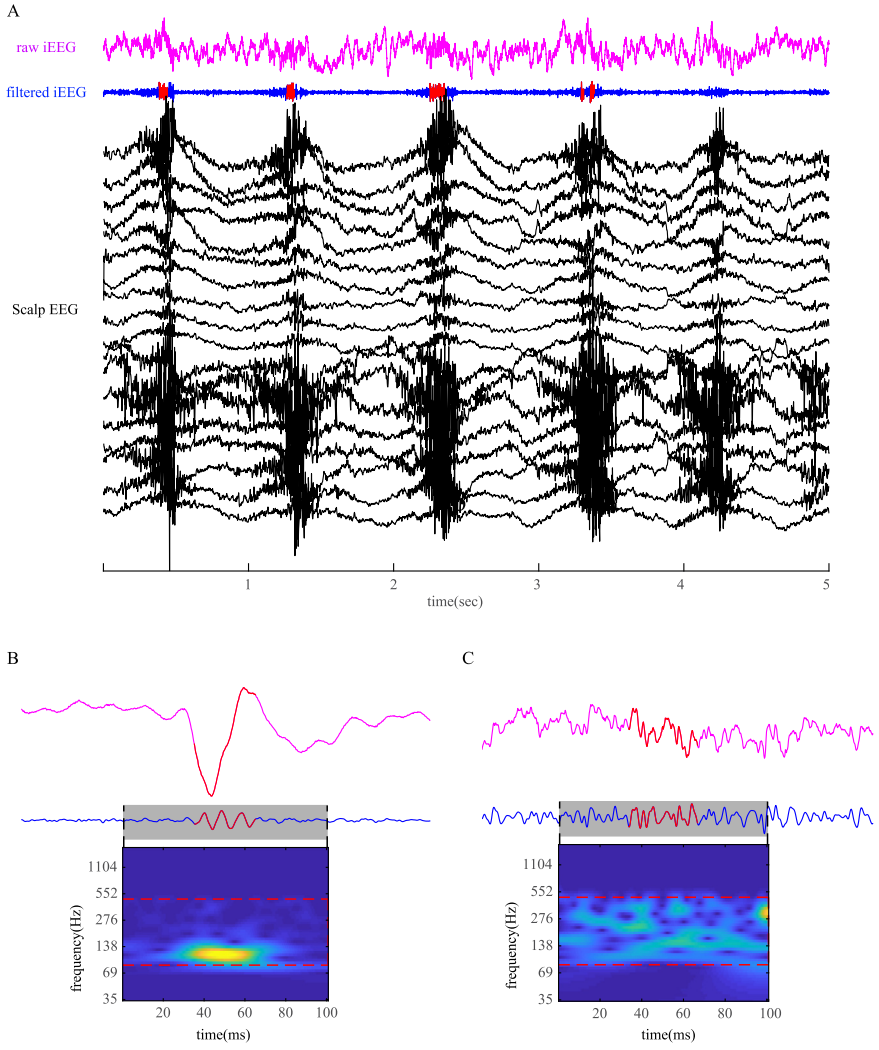

Fig. 2. EMG artifact on intracranial EEG. A: Chewing artifact is readily identified in the scalp (black lines, bottom), but much more subtle intracranially (top). Analyzing the iEEG alone produces waveforms that are detected as potential HFOs by both humans and algorithms (blue lines, with red marks indicating detected "HFOs"). B, C: Expanded view of real HFO (B) and EMG-false-HFO (C), with corresponding time-frequency map derived from wavelet transform (bottom). Values between the red dashed lines (80 and 500 Hz) are used to compute normalized Shannon entropy. Resulting values for these two examples are 8.587(B) and 9.119(C). (For interpretation of the references to color in this figure legend, the reader is referred to the web version of this article.)

2.3.4. Intracranial EMG detector validation

The gold standard for discrimination of EMG-false-HFO was obtained by having a human reviewer blindly label a sample of the detections that had been classified from patients with simultaneous scalp EEG. 2 of the 21 patients were excluded due to technical issues, resulting in 19 patients each contributing an equal number of randomly-selected potential genuine HFOs (200) and EMG-false-HFOs (200), as determined by whether or not they were associated with simultaneous scalp EMG detections (total of 7600 events). The data were displayed as 5 sec waveforms showing the intracranial HFO together with the scalp EEG channels. The reviewer was asked to label each event as either real HFO, EMG-false-HFO, or unclear, based upon the scalp EEG. From these 7600 labelled events, there were 2645 real HFOs, 2262 EMG-false-HFOs, and 2693 unclear events. The number of EMG-false-HFOs for each patient ranged from 0 to 128. We ignored the "unclear" events and compared 2262 detections of each of the other two groups to keep the group sizes equal. These detections were used to evaluate the classification performance in a "leave-one-out" cross-validation analysis, where the data from all but one patient is used to train the classifier, which is then tested on the remaining subject. We also verified that there was no bias in the labeling or classification by calculating the average rate that "unclear" events were classified as EMG-false-HFOs: the average was 0.5 for both the scalp and intracranial algorithms, suggesting lack of systemic bias.

2.4. Image co-registration

We next determined the effect of intracranial location on the prevalence of EMG-false-HFOs. Using a previously developed algorithm (Brang et al., 2016), electrode contacts in the post-implantation CT scan were co-registered to 3-d reconstructed MRI using Freesurfer (Freesurfer 6.0.0). Each ECoG electrode was assigned to the nearest vertex in a mesh model of the patient's pial surface, whereas each depth electrode was assigned to nearest voxel of deep brain structures. 1032 ECoG electrodes and 242 depth electrodes from 20 patients were then mapped onto the Freesurfer average brain to determine the most likely corresponding brain region. Depth electrodes with color-coded artifact rates were presented in semi-transparent images of the average brain. In order to visualize the average susceptibility of ECoG electrode contacts to myogenic contamination, artifact rates were interpolated on the pial surface of the average brain, where each vertex is color coded using the weighted average of the electrodes within a fixed radius ($r^2 = 150\ mm^2$) with the weights calculated using a Gaussian kernel ($sigma^2 = 150\ mm^2$).

We observed that many patients had particularly high levels of EMG-false-HFOs in the temporal lobe channels. We tested whether ECoG electrodes in temporal lobe were correlated with the rate of EMG-false-HFOs with a two-way analysis of variance, with an interaction term included to accommodate individual differences in the spatial distribution of EMG artifacts (using the 'anovan(. . . . . .,'model','interaction')' function in Matlab (Mathworks), independent variables: patient ID, electrode in inferior temporal gyrus or temporal pole according to Destrieux Atlas (Destrieux et al., 2010)). Patients with only depth electrodes implanted are excluded in this analysis, resulting in 14 patients with 1032 ECoG electrodes, of which 125 were classified as one of the temporal locations. MATLAB scripts adapted from iELVis (Groppe et al., 2017) were used for data processing and visualization.

2.5. Effect of EMG artifact rejection on HFO specificity

Two established methods were used to evaluate the clinical significance of HFOs in the context of EZ localization: asymmetry rate and automated identification of seizure onset zone (Gliske et al., 2016). HFO rate asymmetry was used to determine whether redacting muscle artifacts improve the specificity of HFO towards epileptic tissue: it compares the HFO rate inside versus outside a region of interest:

$$A = (r_{in} - r_{out})/(r_{in} + r_{out})$$

Asymmetry ranges from a maximum of 1 (indicating all HFOs are within the identified region) to −1 (all outside the region). A value of 0 indicates the rate is identical inside and outside. Therefore, if HFOs are indicative of epileptic tissue, we expect asymmetry to improve if EMG-false-HFOs are removed from the analysis. We tested asymmetry within two different regions: the clinically-determined seizure onset zone (SOZ) or the resected volume (RV). Note that both of these measurements are only approximations of the true epileptogenic zone (EZ).

The second method analyzes how the new HFO markings might change clinical interpretation. We utilized a previously-validated algorithm that predicts if there are any electrodes likely to be in the EZ (Gliske et al., 2016). Specifically, it looks at the distribution of HFO rates on every channel, performs a kernel density estimation, and determines if there is a distinct population of electrodes with anomalously high HFO rates. Inherent in the method is the ability to avoid choosing any electrodes if none appear to be clearly different than the rest (i.e. it is possible to pick "none"). This algorithm has previously been shown to have high agreement with resected tissue in patients with Class I outcome (Gliske et al., 2016). We compared the results of this algorithm before and after removing the EMG-false-HFOs.

2.6. Data availability

The algorithm and a sample dataset have been uploaded to the journal's data repository. Additional data and code for the previous HFO detector from (Gliske et al., 2016) are available upon request of the authors.

3. Results

3.1. Verification of scalp EMG detector

We assessed the precision and sensitivity of the scalp EMG detection algorithm by comparing its output with human markings. The precision of the EMG detector is computed as the proportion of gold standard (i.e. human-labeled) EMG artifacts compared to all samples in algorithm-labeled EMG samples, whereas the sensitivity is the proportion of algorithm-labeled EMG samples in human-labeled EMG samples. Note that the purpose of the algorithm is to prune HFO detections due to myogenic artifacts rather than to recognize all scalp muscle activity per se, thus the detector is tuned to only detect scalp EMG with amplitude high enough to generate intracranial projections (Fig. 3). Consequently, the automatic EMG detection is precise rather than sensitive (Table 1) when compared with labels of the human reviewer, who was instructed to label all recognizable EMG artifacts in scalp EEG without regard to intracranial HFOs. Of note, the lower sensitivity in UM07 and UM08 was due primarily to prolonged periods of low amplitude, tonic EMG artifact that was unlikely to produce HFOs with our algorithm.

3.2. Verification of the intracranial artifact classifier

The performance of the intracranial artifact rejection algorithm was evaluated in leave-one-out cross validation analysis, done on a per-patient basis. In this case, the algorithm results were assessed

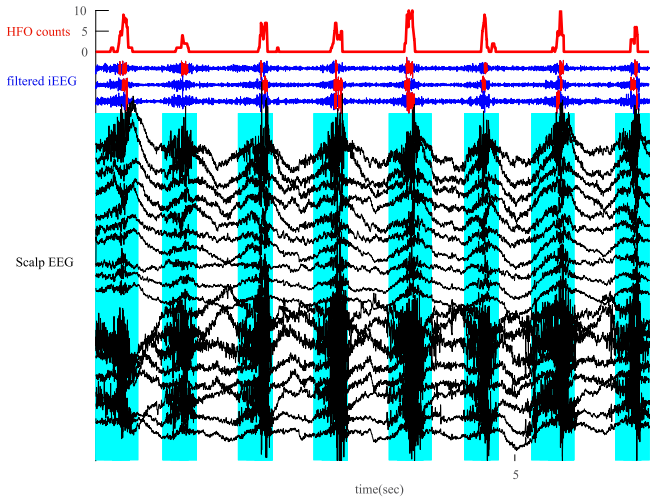

Fig. 3. Scalp EMG detector example. Scalp EEG traces (black lines) show clear EMG artifacts due to chewing, whereas filtered iEEG (80–500 Hz, blue) show possible HFOs (detected HFOs marked with red). The total number of possible HFOs detected across all intracranial electrodes is listed on top as the HFO count (red line). The scalp EMG detector identified periods of EMG artifact across multiple channels (light blue), which can be used to label all detected events in this figure as EMG-false-HFOs. (For interpretation of the references to color in this figure legend, the reader is referred to the web version of this article.)

Table 1
Precision of EMG detector (N = 18,000).

Patient ID	Sensitivity (%)	Precision (%)
UM06	91	99
UM07	42	97
UM08	30	99

against the gold standard of expert human markings that incorporated all EEG channels including the scalp, but the algorithm itself only monitored single channels in intracranial EEG. Fig. 4 shows the results for each of the 18 patients (one patient was excluded in Fig. 4 due to lack of gold-standard to assess the x axis; the y-axis for this patient was 3, i.e. 3% of real HFOs were falsely classified as EMG artifacts), in which all of that patient's data were withheld from the training step then assessed with a cross-validation. As seen in the figure, the combined misclassification rate of both real and EMG-false- HFOs is very low in all patients. As the majority of samples are restricted to the left-lower corner with mean error rates in real HFOs being 0.03 and mean error rates in EMG-false-HFO being 0.06 (sensitivity = 0.94, specificity = 0.97), we concluded that the classifier can be reliably generalized to different subjects. In addition, the boundary used for classification (red line in Fig. 4B) was essentially identical (8.956 ± 0.0033) for all cross validations and for training on the whole data set.

3.3. Spatial characteristics of EMG contamination

We then determined the general rates of EMG-false-HFOs in different brain regions by averaging the rates in each patient in accordance with the 3-D coordinates of each electrode. We combined the results of all intracranial electrodes in 20 patients. The results are shown in Fig. 5, using results from both the scalp EMG detector and the intracranial classifier.

As shown in Fig. 5, both artifact detectors demonstrate that the anterior temporal lobes are particularly susceptible to myogenic contamination. In agreement with visual inspection, two-way ANOVA suggests that anatomical location has significant ($p < 0.001$) influence on the severity of EMG contamination on ECoG electrodes as measured by EMG-false-HFO rate, with anterior and inferior temporal lobe being highly susceptible to muscle activity. This ANOVA accounts for the sample size of each location, and finds that the temporal lobes are more likely to have EMG contamination. In addition, there were significant differences between subjects ($p < 0.001$), with certain individuals having more prominent changes. These between-subject differences appeared to be due to each individual's behavior, as they were not dependent upon type or location of the electrodes. Of note, the depth electrodes showed a clear gradient with proximity to the skull, with exterior electrodes being more severely influenced than interior ones. On average, depth electrodes tend to have higher rates of EMG-artifacts than ECoG electrodes (artifact rates on depth vs. ECoG electrodes are 0.04 ± 0.15 vs. 0.12 ± 0.19 according to intracranial features, or 0.03 ± 0.12 vs. 0.08 ± 0.18 according to scalp EMG detections, correspondingly), while ECoG electrodes have more extreme values at the higher end.

3.4. Clinical significance

Two methods were used to evaluate the clinical impact of EMG-false-HFOs in the context of identifying the EZ. First, we

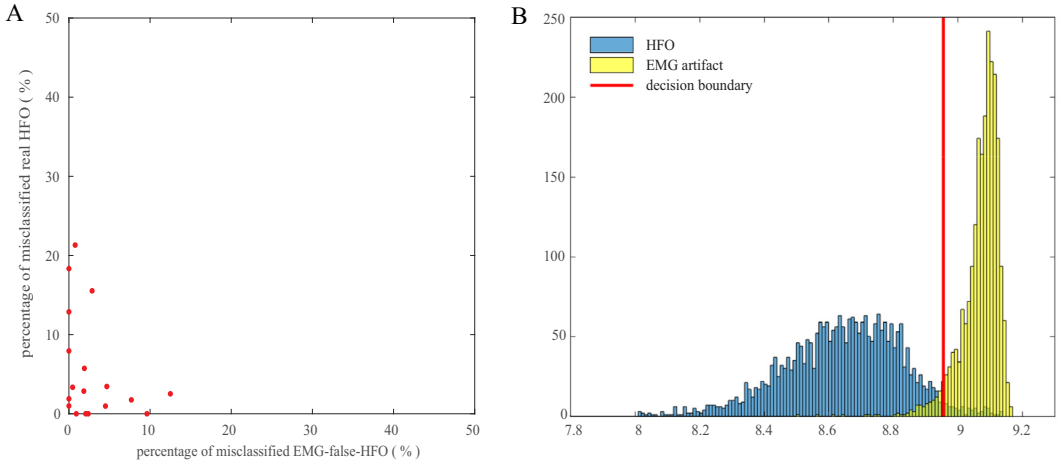

Fig. 4. Intracranial EMG detector validation. A: Error rates (proportion of misclassified events in certain category) for each leave-one-out cross validation, comparing misclassification of both real and EMG-false HFOs, show very good performance of the detector. B: An example of the classifier, in which the wavelet entropy (see Fig. 2B) is very good at distinguishing brain-generated HFOs from EMG-false-HFOs. The boundary to separate them (red line) was determined by training on the entire dataset, which is justified given the similar results in all cross-validations. (For interpretation of the references to color in this figure legend, the reader is referred to the web version of this article.)

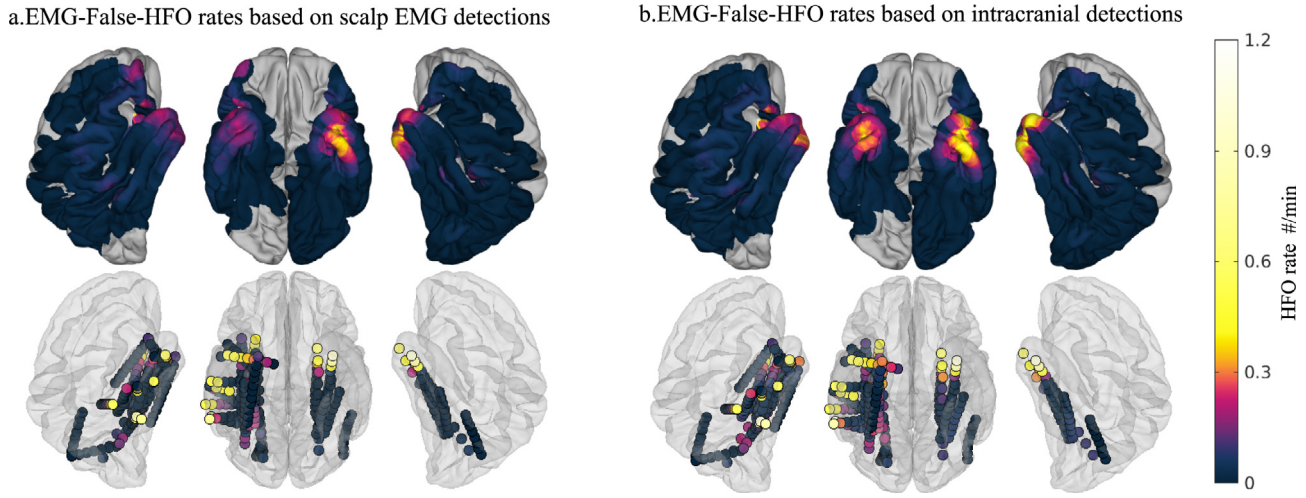

Fig. 5. Spatial location of peak EMG-false-HFOs. A: Scalp EMG detection and B: Intracranial EMG detection both indicate that temporal channels are much more likely to have EMG-false-HFOs. Top rows are based upon grid (ECoG) electrodes, while bottom rows are from depth electrodes. Note the gradient pattern of artifacts rate in concordance with proximity to temporal pole or distance to the skull.

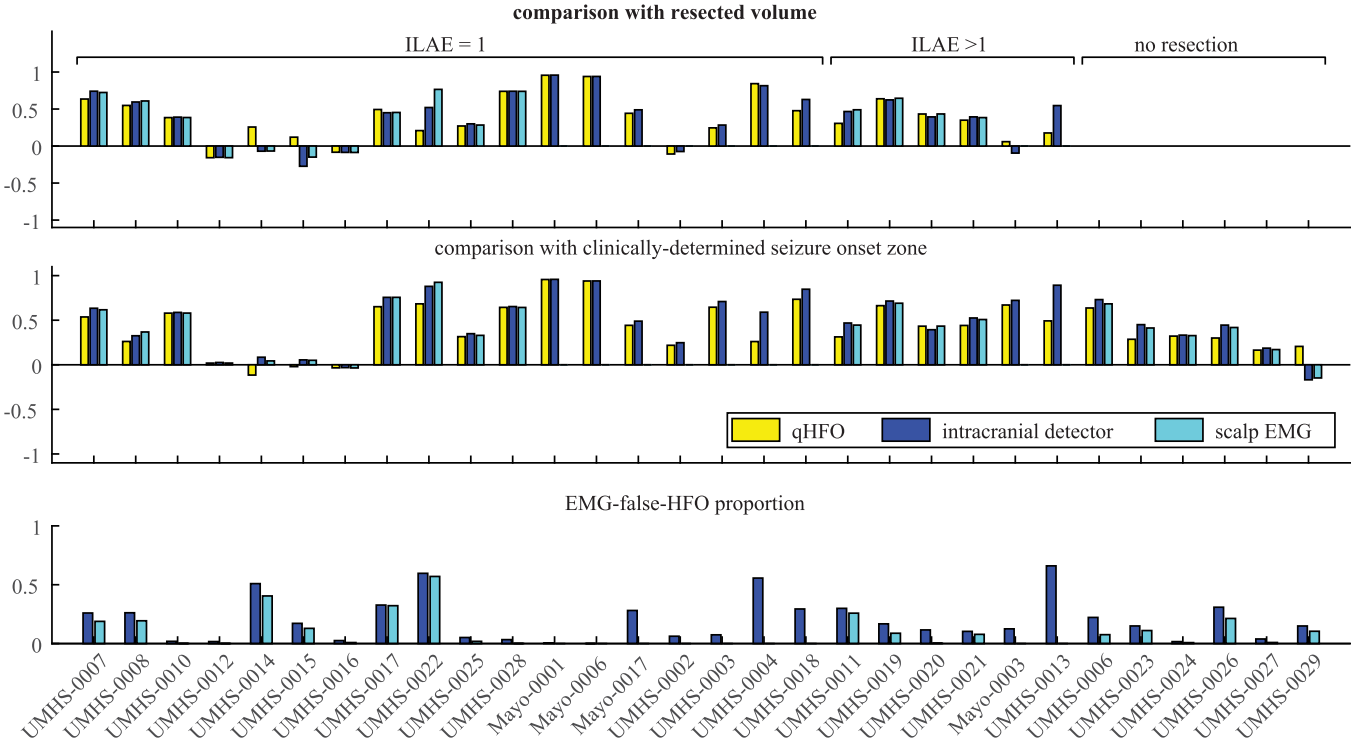

Fig. 6. Clinical effect of EMG artifact rejection. HFO asymmetry with each region of interest (top: RV, middle, SOZ) before and after EMG artifacts rejection. Yellow bars indicate results prior to redaction of EMG-false-HFOs. The intracranial (dark blue) and scalp (light blue) EMG detectors were each assessed independently. Bottom row: proportion of EMG-false-HFO in total qHFO detections. (For interpretation of the references to color in this figure legend, the reader is referred to the web version of this article.)

determined whether redacting muscle artifacts improves the specificity of HFOs towards epileptic tissue measured by HFO rate asymmetry. The asymmetry was measured with respect to both resected volume (RV) and clinically determined seizure onset zone (SOZ), as performed previously (Gliske et al., 2016). Fig. 6 shows asymmetry values for each patient, comparing baseline qHFO detections with the results after applying the two newly-developed artifact rejection methods. Note that some patients did not have scalp EEG available, so the scalp EMG detector was not assessed in those patients. The proportion of EMG-false-HFOs in total qHFO detections is also illustrated, showing large differences between certain patients. Patients with class I outcome were used to assess the significance of the response based on Wilcoxon signed rank test. Both artifact rejection methods significantly increased the HFO asymmetry with SOZ, with the intracranial detector improving results in 18/18 patients ($p = 0.0001$), and scalp-EMG-based method in 9/11 patients ($p = 0.0093$).

When compared with RV, although the intracranial detector produced improvement in 8/17 patients and scalp-EMG based method in 7/11 patients, neither of the responses achieved

statistical significance. This can be partially attributed to the large overlap between resected volume and brain area susceptible to EMG contamination in the temporal lobes, since all patients without increased RV asymmetry underwent temporal lobectomy. In addition, RV usually includes several electrodes that were not identified by the treating clinicians as the SOZ (i.e. the anatomical margins), especially in temporal lobectomies, which disrupts this asymmetry measurement.

Second, we used the output of an algorithm that predicts the location of the Epileptogenic Zone (EZ) based upon high levels of HFOs to demonstrate the effect of muscle contamination related to prospective clinical application. The algorithm was previously validated versus expert human markings to use qHFO detections (which are not designed to avoid EMG-false-HFOs) to identify if there are any electrodes with anomalously high HFO rates, indicative of the EZ (Gliske et al., 2016). The gold standard comparison is to correlate the algorithm prediction with the resected volume (RV) of patients with good outcomes. If successful, we would expect that running this algorithm after removing EMG-false-HFOs would be more specific to the EZ than when it was run with all qHFOs. After removing the putative EMG-false-HFO detections, we re-ran the EZ algorithm on each patient. As shown in Table 2, there were 3 patients (out of 29) in whom redacting EMG-false-HFOs resulted in different predictions from the algorithm. Two of these patients had class one outcome; in one of these the original prediction algorithm was unable to identify any electrodes that clearly had higher HFO rate than the rest. Removing the EMG-false-HFOs then allowed the algorithm to correctly identify electrodes within the EZ—in other words, contamination by muscle activity had generated so many HFOs that it was not possible to identify a subset of abnormally-high channels. In the other patient with good outcome, the original prediction had identified four electrodes correctly within the RV. However, all of these were removed by the muscle artifact rejection, which then selected a separate channel that was also within the RV. The third patient had a class 2 outcome, and originally there was no prediction made. After muscle artifact removal, 4 electrodes were identified as EZ, and only 3 of them were within the RV. While these three results are not enough to prove that clinical results would improve by removing EMG artifacts, they suggest that this algorithm would be an important addition to the care of many patients.

Overall, removing EMG-false-HFOs appears to improve the specificity of HFOs to epileptic tissue in both modalities. Removing them using the scalp EEG algorithm is reliable and easy to verify, and even the intracranial algorithm was able to improve specificity in several patients. The results in Table 2 show that the number of electrodes has some minor changes, but the sensitivity for identifying the RV has not changed significantly, thus the improved specificity was not at the expense of sensitivity. Comparing the two algorithms, we see that the results were similar in all patients except UM 08, in whom the scalp EMG method resulted in two correct predictions while feature-based method generate no prediction.

4. Discussion

Though the conventional wisdom has been that intracranial EEG is relatively unaffected by extracranial bioelectronic sources, our results add to the increasing literature which suggests

Table 2
Predictions of EZ before and after redacting muscle artifacts. Cases where removing EMG-false-HFO resulted in different prediction are highlighted in yellow.

Patient ID	Number of predicted channels within RV / Number of total predicted channels			ILEA outcome
	qHFO	Intracranial detector	Scalp EMG	
Mayo-01	2/2	2/2	Not available	1
Mayo-06	2/2	2/2	Not available	1
Mayo-17	1/1	1/1	Not available	1
UMHS-02	0	0	Not available	1
UMHS-03	0	0	Not available	1
UMHS-04	4/4	1/1	Not available	1
UMHS-07	2/2	2/2	2/2	1
UMHS-08	0	0	2/2	1
UMHS-10	0	0	0	1
UMHS-12	0	0	0	1
UMHS-14	0	0	0	1
UMHS-15	0/2	0/2	0/2	1
UMHS-16	0	0	0	1
UMHS-17	0	0	0	1
UMHS-18	0	0	0	1
UMHS-22	2/2	2/2	2/2	1
UMHS-25	0	0	0	1
UMHS-28	0	0	0	1
UMHS-11	0	0	0	>1
UMHS-19	0	0	0	>1
UMHS-20	0	0	0	>1
UMHS-21	0	0	0	>1
Mayo-03	0/1	0/1	Not available	>1
UMHS-13	0	3/4	Not available	>1
UMHS-06	0	0	0	No resection
UMHS-23	0	0	0	No resection
UMHS-24	0	0	0	No resection
UMHS-26	0	0	0	No resection
UMHS-27	0	0	0	No resection
UMHS-29	0	0	0	No resection

myogenic contamination in intracranial recordings should not be neglected when fast neuronal activity is the subject of investigation. Specifically, the resemblance between HFOs and the intracranial projection of muscle activity poses a unique challenge to HFO research, especially when automatic algorithms are used.

Much research on the relationship between HFOs and epileptogenic zone is done by associating HFO rates in resection volume with the outcome of epilepsy surgery. With the high vulnerability of electrodes near temporal pole to EMG-false-HFOs and temporal lobectomy being the most common type of epilepsy surgery, there exists a risk that HFO detections contaminated with myogenic artifacts may result in artificially inflating the relationship between HFOs and resection volume. By the same token, automatic algorithms may also lead to unreliable conclusions when studying the temporal relationship between HFO occurrence and ictal onsets due to involuntary muscle contractions before and during certain types of seizures.

While most clinical studies have focused on identifying which channels have the highest HFO rates, a longstanding question in HFO research is how to distinguish which HFOs are due to epileptic versus normal brain processes (Engel et al., 2009). Past work has shown that HFOs with higher frequency content (>200 Hz), known as 'fast ripples' may be more specific to epileptic tissue (Staba et al., 2007; van 't Klooster et al., 2017; Wu et al., 2010). The mechanisms producing this fast activity are intriguing, as they appear to require fast firing of many action potentials, indicating a highly active local network (Bragin et al., 2011; Fink et al., 2015; Foffani et al., 2007; Ibarz et al., 2010; Shamas et al., 2018). However, it is not necessary for these phenomena to produce a true coherent oscillation, as the firing cells do not have to be synchronized (Fink et al., 2015; Gliske et al., 2017; Jiruska et al., 2010; Shamas et al., 2018). In terms of detection algorithms, this means that HFOs that are potentially epileptic may have broadband frequency content extending to at least 500 Hz (Blanco et al., 2011; Blanco et al., 2010). Such phenomena are potentially similar to EMG artifacts, which are also characterized by broadband, high frequency content. Thus, it is possible that some "epileptic" HFOs would be classified as EMG-false-HFOs by the intracranial detector. But perhaps more importantly, it is possible that EMG-false-HFOs are falsely classified as "fast ripples." For this reason, it is important to account for EMG contamination when identifying HFOs. There is also the theoretical concern that true fast ripples could be misclassified as EMG artifacts. One potential strategy to address this issue is to set an individualized threshold for the classifier based on information obtained from HFO detections coincident with EMG detections on scalp EEG.

To our knowledge, only one previous study (Otsubo et al., 2008) has addressed the effect of EMG activity on HFO detection. They concluded that muscle contamination occurred only at electrodes close to temporal muscles in their patient. Here, we find that this effect is common in many other patients in both ECoG grid and depth electrodes and is most common in, but not completely restricted to, the electrodes under the temporalis muscle.

Despite the growing interest in adopting automatic algorithms to identify HFOs in long term recordings, the majority of HFO research is restricted to manually identified data during slow wave sleep, where the occurrence of myogenic artifacts is minimized. However, muscle activity can be present in any behavioral state, and automated HFO algorithms should account for this artifact. Standard HFO manual review already usually identifies muscle artifacts, especially in patients that have simultaneous scalp EEG. However, scalp EEG is not always available, and there are significant limitations to the amount of data that can feasibly be analyzed manually. Our algorithm provides a method to analyze the entire EEG automatically and remove EMG artifacts even when scalp EEG is not available, which will greatly expand the amount of HFO data available.

Our results also provide insight on how to recognize EMG-false-HFOs during manual review when scalp recording is not available. EMG-false-HFOs typically contain wide-band spectral power when viewed in time-frequency maps (e.g. Fig. 2), manifesting as the lack of a clear isolated 'island,' as has been suggested previously (Navarrete et al., 2016). However, we also found an additional method that is not as well known: EMG-false-HFOs have time-locked waveforms in more than 2 channels, especially in the most exterior portions of deep electrodes or electrodes close to temporalis muscles. Therefore, we recommend displaying multiple intracranial channels simultaneously to reveal the spatial distribution of HFO-like events, as well as the spectrogram and calculation of wavelet entropy to further assist manual review.

Although both of these algorithms are successful in removing EMG-false-HFO, they each have important limitations. Muscle artifact is very common in some patients on the scalp, sometimes continuing for very long periods; redacting all of these periods can greatly restrict the data available for study, and there are some intracranial electrodes that are unaffected by the artifact. Thus, the scalp EMG detection faces a trade-off between identifying all periods of artifact versus when those artifacts affect intracranial HFO detection. The intracranial algorithm assesses each channel individually without the need of scalp EEG, and has very consistent results in the cross validation. Clearly, the true optimal feature threshold for discriminating EMG-false-HFOs from normal HFO may vary among different subjects due to variance in HFO waveforms and proportion of artifacts in total detections, but these results demonstrate that this algorithm is quite stable across many patients. In addition, the temporal and spatial characteristics may also help differentiating those artifacts from neuronal oscillations. These will be subjects of further investigation.

In conclusion, we have shown that scalp EMG can generate false intracranial HFOs, especially in the temporal region. Care must be taken when evaluating HFOs to avoid these artifacts. We propose that these two algorithms can be used, alone or in concert, to improve the specificity of both automated and manual HFO detections.

Acknowledgements

Research reported in this publication was supported by the National Institute of Health (NIH) [grant numbers R01-NS094399, K01-ES026839 and R00-DC013828]; and Doris Duke Charitable Foundation Clinical Scientist Development Award [grant number 2015096]. We gratefully acknowledge all those involved with obtaining the data, especially G. Worrell and B. Brinkmann at Mayo Clinic.

Disclosure

W.S. and S.G. report a university-sponsored licensing agreement with Natus Medical Incorporated.

References

Benar CG, Chauviere L, Bartolomei F, Wendling F. Pitfalls of high-pass filtering for detecting epileptic oscillations: a technical note on "false" ripples. Clin Neurophysiol 2010;121(3):301–10.

Blanco JA, Stead M, Krieger A, Stacey W, Maus D, Marsh E, et al. Data mining neocortical high-frequency oscillations in epilepsy and controls. Brain 2011;134:2948–59.

Blanco JA, Stead M, Krieger A, Viventi J, Marsh WR, Lee KH, et al. Unsupervised classification of high-frequency oscillations in human neocortical epilepsy and control patients. J Neurophysiol 2010;104(5):2900–12.

Bragin A, Benassi SK, Kheiri F, Engel Jr J. Further evidence that pathologic high-frequency oscillations are bursts of population spikes derived from recordings of identified cells in dentate gyrus. Epilepsia 2011;52(1):45–52.

Brang D, Dai Z, Zheng W, Towle VL. Registering imaged ECoG electrodes to human cortex: A geometry-based technique. J Neurosci Methods 2016;273:64–73.

Crepon B, Navarro V, Hasboun D, Clemenceau S, Martinerie J, Baulac M, et al. Mapping interictal oscillations greater than 200 Hz recorded with intracranial macroelectrodes in human epilepsy. Brain 2010;133:33–45.
Destrieux C, Fischl B, Dale A, Halgren E. Automatic parcellation of human cortical gyri and sulci using standard anatomical nomenclature. Neuroimage 2010;53(1):1–15.
Engel Jr J, Bragin A, Staba R, Mody I. High-frequency oscillations: what is normal and what is not? Epilepsia 2009;50(4):598–604.
Fink CG, Gliske S, Catoni N, Stacey WC. Network mechanisms generating abnormal and normal hippocampal High Frequency Oscillations: a computational analysis. eNeuro 2015;2(3).
Foffani G, Uzcategui YG, Gal B, Menendez de la Prida L. Reduced spike-timing reliability correlates with the emergence of fast ripples in the rat epileptic hippocampus. Neuron 2007;55(6):930–41.
Frauscher B, Bartolomei F, Kobayashi K, Cimbalnik J, van 't Klooster MA, Rampp S, et al. High-frequency oscillations: the state of clinical research. Epilepsia 2017;58(8):1316–29.
Gardner AB, Worrell GA, Marsh E, Dlugos D, Litt B. Human and automated detection of high-frequency oscillations in clinical intracranial EEG recordings. Clin Neurophysiol 2007;118(5):1134–43.
Gliske SV, Irwin ZT, Chestek C, Hegeman GL, Brinkmann B, Sagher O, et al. Variability in the location of high frequency oscillations during prolonged intracranial EEG recordings. Nat Commun 2018;9(1):2155.
Gliske SV, Stacey WC, Lim E, Holman KA, Fink CG. Emergence of narrowband High Frequency Oscillations from asynchronous, uncoupled neural firing. Int J Neural Syst 2017;27(1):1650049.
Gliske SV, Stacey WC, Moon KR, Hero 3rd AO. The intrinsic value of Hfo features as a biomarker of epileptic activity. Proc IEEE Int Conf Acoust Speech Signal Process 2016;2016:6290–4.
Gloss D, Nolan SJ, Staba R. The role of high-frequency oscillations in epilepsy surgery planning. Cochrane Database Syst Rev 2014;1:CD010235.
Groppe DM, Bickel S, Dykstra AR, Wang X, Megevand P, Mercier MR, et al. iELVis: an open source MATLAB toolbox for localizing and visualizing human intracranial electrode data. J Neurosci Methods 2017;281:40–8.
Holler Y, Kutil R, Klaffenbock L, Thomschewski A, Holler PM, Bathke AC, et al. High-frequency oscillations in epilepsy and surgical outcome. A meta-analysis. Front Hum Neurosci 2015;9:574.
Ibarz JM, Foffani G, Cid E, Inostroza M, Menendez de la Prida L. Emergent dynamics of fast ripples in the epileptic hippocampus. J Neurosci 2010;30(48):16249–61.
Jacobs J, Staba R, Asano E, Otsubo H, Wu JY, Zijlmans M, et al. High-frequency oscillations (HFOs) in clinical epilepsy. Prog Neurobiol 2012;98(3):302–15.
Jiruska P, Csicsvari J, Powell AD, Fox JE, Chang WC, Vreugdenhil M, et al. High-frequency network activity, global increase in neuronal activity, and synchrony expansion precede epileptic seizures in vitro. J Neurosci 2010;30(16):5690–701.
Kovach CK, Tsuchiya N, Kawasaki H, Oya H, Howard 3rd MA, Adolphs R. Manifestation of ocular-muscle EMG contamination in human intracranial recordings. Neuroimage 2011;54(1):213–33.
Li A, Chennuri B, Subramanian S, Yaffe R, Gliske S, Stacey W, et al. Using network analysis to localize the epileptogenic zone from invasive EEG recordings in intractable focal epilepsy. Netw Neurosci 2018;2(2):218–40.
Liu S, Sha Z, Sencer A, Aydoseli A, Bebek N, Abosch A, et al. Exploring the time-frequency content of high frequency oscillations for automated identification of seizure onset zone in epilepsy. J Neural Eng 2016;13(2) 026026.
Navarrete M, Alvarado-Rojas C, Le Van Quyen M, Valderrama M. RIPPLELAB: a comprehensive application for the detection, analysis and classification of high frequency oscillations in electroencephalographic signals. PLoS ONE 2016;11(6) e0158276.
Otsubo H, Ochi A, Imai K, Akiyama T, Fujimoto A, Go C, et al. High-frequency oscillations of ictal muscle activity and epileptogenic discharges on intracranial EEG in a temporal lobe epilepsy patient. Clin Neurophysiol 2008;119(4):862–8.
Roehri N, Pizzo F, Bartolomei F, Wendling F, Benar CG. What are the assets and weaknesses of HFO detectors? A benchmark framework based on realistic simulations. PLoS ONE 2017;12(4) e0174702.
Shamas M, Benquet P, Merlet I, Khalil M, El Falou W, Nica A, et al. On the origin of epileptic High Frequency Oscillations observed on clinical electrodes. Clin Neurophysiol 2018;129(4):829–41.
Staba RJ, Frighetto L, Behnke EJ, Mathern GW, Fields T, Bragin A, et al. Increased fast ripple to ripple ratios correlate with reduced hippocampal volumes and neuron loss in temporal lobe epilepsy patients. Epilepsia 2007;48(11):2130–8.
Staba RJ, Wilson CL, Bragin A, Fried I, Engel Jr J. Quantitative analysis of high-frequency oscillations (80–500 Hz) recorded in human epileptic hippocampus and entorhinal cortex. J Neurophysiol 2002;88(4):1743–52.
van 't Klooster MA, van Klink NEC, Zweiphenning W, Leijten FSS, Zelmann R, Ferrier CH, et al. Tailoring epilepsy surgery with fast ripples in the intraoperative electrocorticogram. Ann Neurol 2017;81(5):664–76.
Worrell GA, Gardner AB, Stead SM, Hu S, Goerss S, Cascino GJ, et al. High-frequency oscillations in human temporal lobe: simultaneous microwire and clinical macroelectrode recordings. Brain 2008;131:928–37.
Worrell GA, Jerbi K, Kobayashi K, Lina JM, Zelmann R, Le Van Quyen M. Recording and analysis techniques for high-frequency oscillations. Prog Neurobiol 2012;98(3):265–78.
Wu JY, Sankar R, Lerner JT, Matsumoto JH, Vinters HV, Mathern GW. Removing interictal fast ripples on electrocorticography linked with seizure freedom in children. Neurology 2010;75(19):1686–94.
Zelmann R, Mari F, Jacobs J, Zijlmans M, Dubeau F, Gotman J. A comparison between detectors of high frequency oscillations. Clin Neurophysiol 2012;123(1):106–16.
Zijlmans M, Jiruska P, Zelmann R, Leijten FS, Jefferys JG, Gotman J. High-frequency oscillations as a new biomarker in epilepsy. Ann Neurol 2012;71(2):169–78.